Discrete Transparent Boundary Conditions for transient *kp*–Schrödinger Equations with Application to Quantum–Heterostructures

Andrea Zisowsky[*1], **Anton Arnold**[**2], **Matthias Ehrhardt**[***1], and **Thomas Koprucki**[†3]

[1] Institut für Mathematik, Technische Universität Berlin, Straße des 17. Juni 136, D–10623 Berlin
[2] Institut für Numerische Mathematik, Universität Münster, Einsteinstraße 62, D–48149 Münster
[3] Weierstrass–Institut für Angewandte Analysis und Stochastik, Mohrenstraße 39, D–10117 Berlin

Key words systems of Schrödinger equations, transparent boundary conditions, layered semiconductors, discrete convolution, sum-of-exponentials, finite difference schemes.
MSC (2000) 65M12, 35Q40, 45K05

This work is concerned with *transparent boundary conditions* (TBCs) for *systems of Schrödinger-type equations*, namely the time-dependent *kp-Schrödinger equations*. These TBCs are constructed for the fully discrete scheme (Crank-Nicolson, finite differences), in order to maintain unconditional stability of the scheme and to avoid numerical reflections. The *discrete transparent boundary conditions* (DTBCs) are discrete convolutions in time and are constructed using the $\mathcal{Z}$-transformed solution of the *exterior problem*. We will analyse the numerical error of these convolution coefficients caused by the inverse $\mathcal{Z}$-transformation. Since the DTBCs are non-local in time and thus very costly to evaluate, we present approximate DTBCs of a sum-of-exponentials form that allow for a fast calculation of the boundary terms.

1 Introduction

The operating principle of quantum-electronic semiconductor devices such as resonant tunneling diodes (RTD) [20, Chap. 14] or opto-electronic devices such as quantum-cascade lasers [21] and multi-quantum-well electro-absorption modulators [13] relies on the tunneling process of carriers through barrier structures. Such barrier structures are typically layered semiconductor heterostructures [20], [21], [13] with a barrier thickness of a few nanometers. The transient simulation of wave packets tunneling through such nano-scale semiconductor heterostructures is the key for the understanding of such transport processes [24], [22], [19]. In particular transient simulations can be used to estimate tunneling times [19], charging and escape times [24], [22], or lifetimes of the carriers [13], [23]. For the simulation of the tunneling process usually a scalar Schrödinger equation defined by BenDaniel-Duke-type Hamiltonians [4, Chap. 3] is used [24], [19], [23]. The underlying approximation of the electronic band structure of this type of models is that of a single parabolic band. Parabolic single-band approximations are in good agreement with the real band structure in the vicinity of the minima of the conduction bands, that part of the band structure which is usually occupied by the electrons. For the treatment of the holes, occupying the maxima of the valence bands, the accuracy of parabolic single-band models is often not sufficient. This is mainly due to the fact, that the valence bands possess a much more complex band structure [8], [4], [10], [12], [5], [19], [13]. However, the electronic states of the holes can be approximated well by *multi-band* states which satisfy a so-called *kp-Schrödinger equation*. The time-dependent kp-Schrödinger equation describes the time evolution of the multi-band electronic state and is a *linear coupled system* of Schrödinger equations. The evolution is governed by the kp-Schrödinger operator which as an extension to the single-band models describes a *system* of bands of the band structure, e.g. the four topmost valence bands [4], [10], [12], [5]. There exists a whole bunch of such multi-band kp-models [17] including also combined models for conduction and valence bands. The latter also allow for a non-parabolic approximation of the conduction bands. For devices where the parabolic conduction band approximation is not sufficient such kp-models can be used. For unipolar devices where by crossing a barrier a conduction-band to valence-band transition is possible such as *resonant interband tunneling diodes* (RITD) or for bipolar devices where additionally the hole tunneling processes are important such as multi-quantum well electro-absorption modulators multi-band modeling is necessary. In these cases the numerical solution of the time-dependent kp-Schrödinger equation can be used to understand and to determine the tunneling properties of corresponding semiconductor heterostructures by studying the time evolution of the multi-band electronic state.

In this paper we are concerned with the numerical treatment of a time-dependent system of kp-Schrödinger-type. Such type of linear systems of Schrödinger equations also arise as "parabolic systems" in electromagnetic wave propagation. In both cases artificial boundary conditions (BCs) have to be imposed to restrict the unbounded domain, on which the differential

* Corresponding author: e-mail: zisowsky@math.tu-berlin.de
** e-mail: anton.arnold@math.uni-muenster.de.
*** e-mail: ehrhardt@math.tu-berlin.de.
† e-mail: koprucki@wias-berlin.de.

equation is originally defined, to a finite computational domain. Such BCs are called *transparent boundary conditions* (TBCs), if the solution on the whole space (restricted to the computational domain) is equal to the solution with the artificial BCs. The artificial boundary splits the problem into three parts: the interesting interior problem and a left and right exterior problem. For constant coefficients the exterior problems can be solved explicitly by the Laplace method. Assuming (spatial) C^1-continuity of the solution at the artificial boundaries yields the TBC as a Dirichlet–to–Neumann map [1], [14]. An ad-hoc discretisation of these continuous TBC can destroy the stability of the employed numerical scheme for the PDE and induce numerical reflections. To avoid this, we derive *discrete TBCs* (DTBCs) for the fully discretised PDE. The procedure is analogous to the continuous case and uses the $\mathcal{Z}$-transformation. The inverse Laplace/$\mathcal{Z}$-transformation yields a convolution in time. Hence, the perfectly *exact* BC is non-local in time and therefore very costly for long–time simulations. To reduce the numerical effort, we introduce approximate DTBCs. Since the inverse $\mathcal{Z}$-transformation must be accomplished numerically for Schrödinger–type systems, an additional small numerical error is induced.

The paper is organised as follows: Sect. 2 introduces the system of kp-Schrödinger equations and presents a quantum well structure with a double barrier as an example that will be considered throughout this work. We derive the analytic TBC in Sect. 3 and its discrete version in Sect. 4. Here, we also scrutinise the coefficients of the discrete convolution. We then explain our strategy to compute the coefficients by a numerical inverse $\mathcal{Z}$-transformation in Sect. 5 and discuss its numerical error. In Sect. 6 we approximate the coefficients by a sum-of-exponentials ansatz and present a fast evaluation of the approximate DTBC. Finally, in Sect. 7 we present numerical simulations for a quantum–heterostructure.

2 The System of *kp*-Schrödinger Equations

We consider a system of *Schrödinger-type equations* in one space dimension, namely the kp-Schrödinger equation for one-dimensional semiconductor nanostructures. They are layered *heterostructures* consisting of layers of different semiconductor materials with abrupt, planar heterojunction interfaces between the layers [20]. Typical examples are semiconductor quantum wells and double-barrier structures [20], [4], [12]. A widely used approach for the modeling of the near-band-edge electronic states in semiconductor nanostructure is the kp-method [15] in combination with the envelope function approximation [4], [6], [7]. Within this approach the electronic state $\Psi(\mathbf{r})$ is approximated in terms of d bands

$$\Psi_{\mathbf{k}_\parallel}(\mathbf{r}) = \exp(\mathrm{i}\mathbf{k}_\parallel \cdot \mathbf{r}_\parallel) \sum_{\nu=1}^{d} \varphi_\nu(x;\mathbf{k}_\parallel) u_{\nu,\mathbf{k}=\mathbf{0}}(\mathbf{r}) \qquad \text{with } \mathbf{r} = (\mathbf{r}_\parallel, x) \in \mathbb{R}^3 .$$

The index $\parallel$ indicates in-plane vectors and x denotes the growth direction of the semiconductor layers. $\mathbf{k}_\parallel = (k_1, k_2) \in \mathbb{R}^2$ is the reduced wave vector, which will be fixed for each simulation model. $u_{\nu,\mathbf{k}=\mathbf{0}}(\mathbf{r})$ are lattice periodic, zone-center Bloch functions varying on the atomic scale and $\varphi_\nu(x;\mathbf{k}_\parallel)$ are the corresponding envelope functions describing the variation of the wave function on the (larger) nanoscale. The vector of the envelope functions $\boldsymbol{\varphi} = (\varphi_1, \cdots, \varphi_d)$ with $\boldsymbol{\varphi}(x,t) \in \mathbb{C}^d$ fulfill the one-dimensional *kp-Schrödinger equation*

$$\mathrm{i}\frac{\partial}{\partial t}\boldsymbol{\varphi} = \mathbf{H}\Big(\mathbf{k}_\parallel, -\mathrm{i}\frac{\partial}{\partial x}\Big)\boldsymbol{\varphi} .$$

There is a hierarchy of kp-models [17] including 4-band, 6-band and 8-band Hamiltonians. Depending on the model Hamiltonian, effects such as quantum confinement, band-mixing, spin-orbit interaction and mechanical strain can be treated consistently. The basic stage in this model hierarchy is the 4×4 Luttinger-Kohn-Hamiltonian which describes the band-mixing between the heavy holes and the light holes [4], [11], [10], [12].

In notation we follow [3] and write the system as

$$\mathrm{i}\frac{\partial}{\partial t}\boldsymbol{\varphi} = -\frac{\partial}{\partial x}(\mathbf{m}(x)\frac{\partial}{\partial x}\boldsymbol{\varphi}) + \mathbf{M}_S(x)\frac{\partial}{\partial x}\boldsymbol{\varphi} - \frac{\partial}{\partial x}(\mathbf{M}_S^H(x)\boldsymbol{\varphi}) + \mathbf{V}(x)\boldsymbol{\varphi}, \quad x \in \mathbb{R}, t > 0 , \tag{1}$$

with

$$\mathbf{M}_S(x) := \mathbf{M}_0(x) + k_1\mathbf{M}_1(x) + k_2\mathbf{M}_2(x), \quad \mathbf{V}(x) := k_1\mathbf{U}_1(x) + k_2\mathbf{U}_2(x) + \sum_{\alpha\beta} k_\alpha k_\beta \mathbf{U}_{\alpha\beta}(x) + \mathbf{v}(x) + \mathbf{e}(x),$$

where the mass matrix $\mathbf{m}(x)$ is real and diagonal. $\mathbf{M}_S(x) \in \mathbb{C}^{d\times d}$ is skew-Hermitian, and $\mathbf{V}(x) \in \mathbb{C}^{d\times d}$ is Hermitian. The real diagonal matrix $\mathbf{e}(x)$ describes the variation of the band-edges. The band-mixing due to the kp-interaction of the first and second order are described by the terms containing the matrices $\mathbf{M}_\alpha, \mathbf{U}_\alpha, \alpha = 0, 1, 2$, and $\mathbf{U}_{\alpha\beta}, \alpha, \beta = 1, 2$, respectively. The potential $\mathbf{v}$ can cover couplings induced by the spin-orbit interaction or by mechanical strain. When neglecting all non-diagonal coupling terms, the system would reduce to an uncoupled system of scalar Schrödinger equations corresponding to the case of uncoupled parabolic bands. In this sense the couplings can be interpreted as correction terms to the parabolic band structure approximation.

Due to its Hamiltonian structure, the system (1) clearly preserves $||\boldsymbol{\varphi}||_{L^2}^2$ in time (conservation of mass).

2.1 The Double-Barrier Stepped Quantum-Well Structure

We now introduce an example that we will use throughout this work to illustrate the numerical results. We consider the *$GaAs/AlGaAs$ double-barrier stepped quantum-well structure* (DBSQW) introduced in [24]. The variation of the band-edges $e(x)$ is depicted in Fig. 1. For this kind of structure an analysis of the time evolution of wave packets tunneling through the structure has been performed using a scalar Schrödinger equation [24]. We consider the more accurate four-band Luttinger-Kohn-Hamiltonian [4], [11], [10], [12] modeling the band-mixing of heavy and light holes. In atomic units adapted to the light holes ($\hbar = 1$, $m_0/(\gamma_1 + 2\gamma_2) = 1$) the coefficient matrices for the corresponding 4×4 system of Schrödinger equations are given by $\mathbf{m} = 0.5 \cdot \mathrm{diag}(\gamma, 1, 1, \gamma)\,, \mathbf{M}_0 = \mathbf{0}$,

$$\mathbf{M}_1 = \frac{1}{2}\frac{\gamma_3}{\gamma_1+2\gamma_2}\sqrt{3}\mathrm{i}\begin{pmatrix} 0 & 1 & 0 & 0 \\ 1 & 0 & 0 & 0 \\ 0 & 0 & 0 & -1 \\ 0 & 0 & -1 & 0 \end{pmatrix}, \qquad \mathbf{M}_2 = \frac{1}{2}\frac{\gamma_3}{\gamma_1+2\gamma_2}\sqrt{3}\begin{pmatrix} 0 & 1 & 0 & 0 \\ -1 & 0 & 0 & 0 \\ 0 & 0 & 0 & -1 \\ 0 & 0 & 1 & 0 \end{pmatrix},$$

$$\mathbf{U}_{11,\,22} = \frac{1}{2}\frac{1}{\gamma_1+2\gamma_2}\begin{pmatrix} \gamma_1+\gamma_2 & 0 & \mp\sqrt{3}\gamma_2 & 0 \\ 0 & \gamma_1-\gamma_2 & 0 & \mp\sqrt{3}\gamma_2 \\ \mp\sqrt{3}\gamma_2 & 0 & \gamma_1-\gamma_2 & 0 \\ 0 & \mp\sqrt{3}\gamma_2 & 0 & \gamma_1+\gamma_2 \end{pmatrix}, \qquad \mathbf{U}_{12}+\mathbf{U}_{21} = \frac{\sqrt{3}\gamma_3\mathrm{i}}{\gamma_1+2\gamma_2}\begin{pmatrix} 0 & 0 & 1 & 0 \\ 0 & 0 & 0 & 1 \\ -1 & 0 & 0 & 0 \\ 0 & -1 & 0 & 0 \end{pmatrix},$$

and $\mathbf{U}_1 = \mathbf{U}_2 = \mathbf{0}$ with $\gamma = \frac{\gamma_1-2\gamma_2}{\gamma_1+2\gamma_2}$. The values of the band structure parameters for $GaAs$ are given by $\gamma_1 = 6.85$, $\gamma_2 = 2.1$, $\gamma_3 = 2.9$. For the in-plane wave-vector $\mathbf{k}_\parallel$ we choose $k_1 = 2.3$, $k_2 = 0$. As initial condition we use a Gaussian wave packet

$$\boldsymbol{\varphi}(x,0) = (2\pi\sigma^2)^{\frac{1}{4}} \exp\left(\mathrm{i}k_r x - \frac{(x-x_0)^2}{\sigma^2}\right) \cdot \zeta\,, \tag{2}$$

where $\zeta \in \mathbb{C}^d$ is a linear combination of eigenmodes calculated via the dispersion relation of (1) and $\sigma = 3$, $x_0 = -2\sigma$ and $k_r = \sqrt{6.99}$. The band-edge profile $\mathbf{e}(x) = e(x)\mathbf{I}$ (with the identity matrix $\mathbf{I}$) of the DBSQW is taken from [24] and defined by (3).

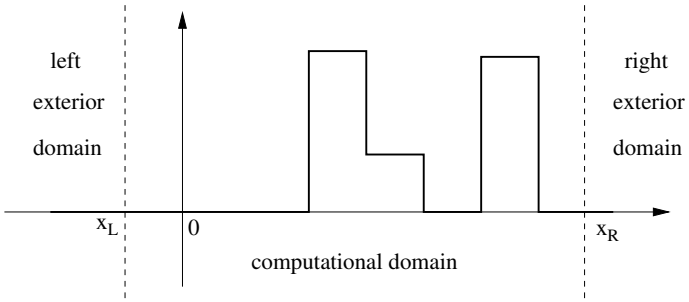

$$e(x) = \begin{cases} 0, & x \le 0 \\ \frac{15}{2}, & 0 < x \le 0.5 \\ \frac{3}{2}, & 0.5 < x \le 1 \\ 0, & 1 < x \le 1.5 \\ \frac{15}{2}, & 1.5 < x \le 2 \\ 0, & 2 < x \end{cases}. \tag{3}$$

Fig. 1 Variation of the band-edge $e(x)$ for the $GaAs/AlGaAs$ DBSQW structure.

The computational domain is now defined such that it contains the *significant* part of the initial data and the x-dependent part of the band-edge potential (cf. Fig. 1). Therefore, we introduce in Sec. 3 TBCs at the left and right boundary $x = x_L$ and $x = x_R$.

3 The Transparent Boundary Conditions

We will now derive the analytic TBCs for the kp-Schrödinger equation (1). In the scalar case (classical Schrödinger equation), the Laplace-transformed equation (a linear second order ODE) in the exterior domain can be solved explicitly. Afterwards, the solution is inverse transformed, thus yielding the analytic TBC (cf. [1]). For systems of equations the inverse Laplace transform, in general, cannot be calculated explicitly. Nevertheless, we will present the derivation of the Laplace transformed TBC.

For the derivation we consider the Schrödinger equation in the left/right exterior domain. A Laplace transformation yields a system of ordinary differential equations, whose solution can be given in terms of its eigenvalues and eigenvectors. We will prove that half of the eigenvalues have positive real parts and thus yield solutions increasing for $x \to \infty$; the other half has negative real parts, yielding decreasing solutions. Demanding that the increasing solutions vanish in the exterior domains leads to the TBCs.

We consider equation (1) in the bounded domain $[x_L, x_R]$ together with TBCs at $x = x_L$ and $x = x_R$. We will denote the constant parameter matrices in the left and right exterior problem by a superscript L and R, respectively, when we need to distinguish between the boundaries. But since the derivation for the left and right TBC is analogous, we focus on the

right boundary and omit the superscript R until needed. The TBC at $x = x_R$ is constructed by considering (1) with constant coefficients for $x > x_R$, the so-called *right exterior problem*

$$\mathrm{i}\boldsymbol{\varphi}_t = -\mathbf{m}\boldsymbol{\varphi}_{xx} + \mathrm{i}\mathbf{M}\boldsymbol{\varphi}_x + \mathbf{V}\boldsymbol{\varphi}, \qquad x > x_R,\ t > 0, \tag{4}$$

where all coefficient matrices are constant, $\mathbf{M} = \mathbf{M}^H = -\mathrm{i}(\mathbf{M}_S - \mathbf{M}_S^H)$, and$\mathbf{V} = \mathbf{V}^H$. The mass matrix $\mathbf{m}$ is diagonal, and we shall henceforth assume that it is regular.

We now use the Laplace-transformation given by $\hat{\boldsymbol{\varphi}}(x,s) = \int_0^\infty \mathrm{e}^{-st}\boldsymbol{\varphi}(x,t)\,dt\,, \quad s = \alpha + \mathrm{i}\xi\,, \quad \alpha > 0\,, \quad \xi \in \mathbb{R}$ and obtain from (4) the *transformed right exterior problem*

$$\mathbf{m}\hat{\boldsymbol{\varphi}}_{xx} - \mathrm{i}\mathbf{M}\hat{\boldsymbol{\varphi}}_x = (\mathbf{V} - \mathrm{i}s\mathbf{I})\hat{\boldsymbol{\varphi}}\,, \qquad x > x_R\,, \tag{5}$$

which is uniquely solvable:

Lemma 3.1 *Let Re*$(s) > 0$*. Then, the BVP* (5) *with the boundary conditions*

$$\hat{\boldsymbol{\varphi}}(x = x_R) = \hat{\boldsymbol{\Phi}} \in \mathbb{C}^d\,, \qquad \hat{\boldsymbol{\varphi}}(x = \infty) = \mathbf{0} \tag{6}$$

has a unique (classical) solution.

Proof. W.r.o.g. we put $x_R = 0$ and set $\tilde{\boldsymbol{\varphi}}(x) := \hat{\boldsymbol{\varphi}}(x) - \hat{\boldsymbol{\Phi}}e^{-x}$, $x > 0$ to transform the BVP to homogeneous boundary data:

$$(\mathbf{L} - is\mathbf{I})\tilde{\boldsymbol{\varphi}}(x) = \mathbf{g}(x) := (\mathbf{m} + i\mathbf{M} - \mathbf{V} + is\mathbf{I})\hat{\boldsymbol{\Phi}}e^{-x} \qquad \in L^2(\mathbb{R}^+;\mathbb{C}^d)\,, \tag{7}$$

with the operator $\mathbf{L} := -\mathbf{m}\partial_x^2 + i\mathbf{M}\partial_x + \mathbf{V}$ defined on $\mathcal{D}(\mathbf{L}) = H^2(\mathbb{R}^+) \cap H_0^1(\mathbb{R}^+)$. Since $-\mathbf{m}\partial_x^2$ is self-adjoined on $\mathcal{D}(\mathbf{L})$, so is $\mathbf{L}$ (due to the Kato-Rellich theorem) since the lower order terms of $\mathbf{L}$ are *infinitesimally small* with respect to $-\mathbf{m}\partial_x^2$ (cf. [18, Chap. 10]). Hence, $is \in \rho(\mathbf{L})$, the resolvent set of $\mathbf{L}$, and (7) has a unique solution $\tilde{\boldsymbol{\varphi}} \in \mathcal{D}(\mathbf{L})$. □

The linear Dirichlet-to-Neumann map $\hat{\boldsymbol{\Phi}} \mapsto \hat{\boldsymbol{\varphi}}_x(x_R)$ will be the Laplace-transformed TBC that we seek.

We shall next derive an explicit form of this TBC which is useful for numerical purposes. We define $\boldsymbol{\nu} = \hat{\boldsymbol{\varphi}}$ and $\boldsymbol{\eta} = \hat{\boldsymbol{\varphi}}_x$ and thus obtain a system of first order differential equations

$$\underbrace{\begin{pmatrix} \mathbf{M} & \mathrm{i}\mathbf{m} \\ -\mathrm{i}\mathbf{m} & \mathbf{0} \end{pmatrix}}_{\mathbf{A}} \begin{pmatrix} \boldsymbol{\nu}_x \\ \boldsymbol{\eta}_x \end{pmatrix} = \underbrace{\begin{pmatrix} \mathrm{i}\mathbf{V} + s\mathbf{I} & \mathbf{0} \\ \mathbf{0} & -\mathrm{i}\mathbf{m} \end{pmatrix}}_{\mathbf{B}} \begin{pmatrix} \boldsymbol{\nu} \\ \boldsymbol{\eta} \end{pmatrix}\,, \qquad x > x_R\,. \tag{8}$$

It can easily be shown that the matrix $\mathbf{A}$ is regular with the inverse

$$\mathbf{A}^{-1} = \mathbf{m}^{-1}\begin{pmatrix} \mathbf{0} & \mathrm{i}\mathbf{I} \\ -\mathrm{i}\mathbf{I} & -\mathbf{M}\mathbf{m}^{-1} \end{pmatrix} \text{ and } \mathbf{A}^{-1}\mathbf{B} = \begin{pmatrix} \mathbf{0} & \mathbf{I} \\ \mathbf{m}^{-1}(\mathbf{V} - \mathrm{i}s\mathbf{I}) & \mathrm{i}\mathbf{m}^{-1}\mathbf{M} \end{pmatrix}\,. \tag{9}$$

Also $\mathbf{B}$ (and hence also $\mathbf{A}^{-1}\mathbf{B}$) is regular for $\mathrm{Re}(s) > 0$, since it is a block diagonal matrix with regular block matrices on the diagonals ($\mathbf{V}$ is Hermitian and thus it is diagonalisable with real eigenvalues).

We now transform $\mathbf{A}^{-1}\mathbf{B}$ into Jordan form with $\mathbf{A}^{-1}\mathbf{B} = \mathbf{P}\mathbf{J}\mathbf{P}^{-1}$, where $\mathbf{P}^{-1}$ contains the left eigenvectors in rows. We sort the Jordan blocks in $\mathbf{J}$ with respect to an increasing real part of the corresponding eigenvalue. Thus, $\mathbf{J}$ can be written as $\mathbf{J} = \left(\begin{smallmatrix} \mathbf{J}_1 & \mathbf{0} \\ \mathbf{0} & \mathbf{J}_2 \end{smallmatrix}\right)$, where $\mathbf{J}_1$ holds all Jordan blocks to eigenvalues with negative real parts and $\mathbf{J}_2$ those with positive real parts. Due to Thm. 3.2 $\mathbf{J}_1$ and $\mathbf{J}_2$ are $d \times d$-matrices. With $\mathbf{P}^{-1} = \left(\begin{smallmatrix} \mathbf{P}_1 & \mathbf{P}_2 \\ \mathbf{P}_3 & \mathbf{P}_4 \end{smallmatrix}\right)$ equation (8) can be written as

$$\mathbf{P}^{-1}\begin{pmatrix} \boldsymbol{\nu}_x \\ \boldsymbol{\eta}_x \end{pmatrix} = \begin{pmatrix} \mathbf{J}_1 & \mathbf{0} \\ \mathbf{0} & \mathbf{J}_2 \end{pmatrix}\begin{pmatrix} \mathbf{P}_1 & \mathbf{P}_2 \\ \mathbf{P}_3 & \mathbf{P}_4 \end{pmatrix}\begin{pmatrix} \boldsymbol{\nu} \\ \boldsymbol{\eta} \end{pmatrix} = \begin{pmatrix} \mathbf{J}_1 & \mathbf{0} \\ \mathbf{0} & \mathbf{J}_2 \end{pmatrix}\begin{pmatrix} \mathbf{P}_1\boldsymbol{\nu} + \mathbf{P}_2\boldsymbol{\eta} \\ \mathbf{P}_3\boldsymbol{\nu} + \mathbf{P}_4\boldsymbol{\eta} \end{pmatrix}\,, \qquad x > x_R\,. \tag{10}$$

Obviously, the upper equation yields the solution components, which decrease for $x \to \infty$ and the lower equation yields the increasing parts. We define the *left exterior problem* for $x < x_L$ analogously to the right exterior problem. Then, an equation analogous to (10) holds: the *transformed TBCs* for the left and right boundary are obtained by extinguishing the increasing parts of the exterior solutions:

$$\mathbf{P}_2^L\hat{\boldsymbol{\varphi}}_x(x_L,s) = -\mathbf{P}_1^L\hat{\boldsymbol{\varphi}}(x_L,s)\,, \qquad \mathbf{P}_4^R\hat{\boldsymbol{\varphi}}_x(x_R,s) = -\mathbf{P}_3^R\hat{\boldsymbol{\varphi}}(x_R,s)\,. \tag{11}$$

If the matrices $\mathbf{P}_2^L$ and $\mathbf{P}_4^R$ are regular, then the Laplace-transformed TBC can be written in *Dirichlet-to-Neumann form*. It is not clear, if these matrices are regular in general, but for our example this applied for all tested values of s.

In order to understand the structure of increasing and decaying solutions of (5), we state the following theorem:

Theorem 3.2 (Splitting Theorem) *For Re$(s) > 0$ the regular matrix $\mathbf{A}^{-1}\mathbf{B}$ has d eigenvalues with positive real part and d with negative real part.*

The proof of this theorem will be obtained as a conclusion of Lem. 3.3 and Lem. 3.4. We first recall the definition of the *inertia* of a matrix $\mathbf{M}$:

Definition 1 The *inertia* of a complex matrix $\mathbf{M}$ is the ordered triple $i(\mathbf{M}) = (i_+(\mathbf{M}), i_-(\mathbf{M}), i_0(\mathbf{M}))$, where $i_+(\mathbf{M})$, $i_-(\mathbf{M})$ and $i_0(\mathbf{M})$ are the numbers of eigenvalues of $\mathbf{M}$ with resp. positive, negative and zero real part, all counting multiplicity.

Lemma 3.3 (Lemma 2 in [9]) *Let $\mathbf{F}, \mathbf{G}$ be $d \times d$-matrices with $\mathbf{G}$ Hermitian and regular, suppose $\mathbf{H} := \mathbf{GF} + \mathbf{F}^H\mathbf{G}$ is positive semi-definite and $i_0(\mathbf{F}) = 0$. Then $i(\mathbf{F}) = i(\mathbf{G})$.*

In order to apply this lemma to $\mathbf{G} := \mathbf{A}$ and $\mathbf{F} := \mathbf{A}^{-1}\mathbf{B}$ we check the assumptions: Since $\mathbf{M}$ is Hermitian, $\mathbf{A} = \mathbf{A}^H$ as well. We already noted that $\mathbf{A}$ is regular. Then $\mathbf{H}$ satisfies:

$$\mathbf{H} \;=\; \mathbf{GF} + \mathbf{F}^H\mathbf{G} = \mathbf{A}(\mathbf{A}^{-1}\mathbf{B}) + \mathbf{B}^H(\mathbf{A}^{-1})^H\mathbf{A}^H = \mathbf{B} + \mathbf{B}^H = \begin{pmatrix} 2\mathrm{Re}(s)\mathbf{I} & \mathbf{0} \\ \mathbf{0} & \mathbf{0} \end{pmatrix} \geq 0.$$

It remains to show, that $i_0(\mathbf{A}^{-1}\mathbf{B}) = 0$. To this end we prove the following lemma:

Lemma 3.4 *For Re$(s) > 0$ the matrix $\mathbf{A}^{-1}\mathbf{B}$ has no purely imaginary eigenvalues.*

Proof. We assume that $\mathrm{i}\lambda$ with $\lambda \in \mathbb{R}$ is eigenvalue of $\mathbf{A}^{-1}\mathbf{B}$. In that case $\hat{\boldsymbol{\varphi}}(x) = \check{\boldsymbol{\varphi}}\mathrm{e}^{\mathrm{i}\lambda x}$ is a solution of (5) and yields $is\check{\boldsymbol{\varphi}} = (\mathrm{i}\alpha - \xi)\check{\boldsymbol{\varphi}} = (\mathbf{m}\lambda^2 - \mathbf{M}\lambda + \mathbf{V})\check{\boldsymbol{\varphi}}$ for $s = \alpha + \mathrm{i}\xi$. Hence, $\mathrm{i}\alpha - \xi$ is an eigenvalue of the Hermitian matrix $\mathbf{m}\lambda^2 - \mathbf{M}\lambda + \mathbf{V}$. Therefore $\alpha = 0$ which is a contradiction. □

Conclusion 1 For any eigenvalue λ of $\mathbf{A}^{-1}\mathbf{B}$, $\mathrm{Re}(\lambda) = 0$ implies $\lambda = 0$. Thus, since $\mathbf{A}^{-1}\mathbf{B}$ is regular, we have $i_0(\mathbf{A}^{-1}\mathbf{B}) = 0$.

Hence, Lem. 3.3 applies and yields $i(\mathbf{A}^{-1}\mathbf{B}) = i(\mathbf{A})$. To prove Thm. 3.2, it finally remains to verify that d eigenvalues of $\mathbf{A}$ are positive and d are negative. To this end we will use a continuity argument: we consider the matrix

$$\mathbf{A}(\varepsilon) := \begin{pmatrix} \varepsilon\mathbf{M} & \mathrm{i}\mathbf{m} \\ -\mathrm{i}\mathbf{m} & \mathbf{0} \end{pmatrix}, \qquad \varepsilon \in [0,1]\,.$$

$\mathbf{A}(0)$ has d positive and d negative eigenvalues, which are given by $\lambda^0_{2k-1} = m_{k,k}$ and $\lambda^0_{2k} = -m_{k,k}$, $k = 1, \ldots, d$. Furthermore, for all $\varepsilon \in [0,1]$ the matrix $\mathbf{A}(\varepsilon)$ has no zero eigenvalue (cp. to (9)). Then, for ε from zero to one d eigenvalues of $\mathbf{A}(\varepsilon)$ are positive and d are negative, since the eigenvalues are continuous in ε. Thus, $i(\mathbf{A}) = (d, d, 0)$ holds and Lem. 3.3 implies $i(\mathbf{A}^{-1}\mathbf{B}) = (d, d, 0)$, if $\mathrm{Re}(s) > 0$, which finishes the proof of Thm. 3.2.

4 The Discrete Transparent Boundary Conditions

We do not discretise the analytic BC (11) (by a numerical inverse Laplace transformation), but derive DTBCs for a full discretisation of the whole–space problem (1). For the discretisation we choose a uniform grid with the step sizes Δx in space and Δt in time: $x_j = x_L + j\Delta x, t_n = n\Delta t$ with $j \in \mathbb{Z}$, $n \in \mathbb{N}_0$. We use a Crank-Nicolson scheme in time and central differences for the first and second spatial derivatives. The *discrete kp-Schrödinger equation* then reads

$$\mathrm{i}\frac{\Delta x^2}{\Delta t}(\boldsymbol{\varphi}_j^{n+1} - \boldsymbol{\varphi}_j^n) = -\Delta^0_{\frac{\Delta x}{2}}(\mathbf{m}_j\Delta^0_{\frac{\Delta x}{2}}\boldsymbol{\varphi}_j^{n+\frac{1}{2}}) + \frac{\Delta x}{2}\left(\mathbf{M}_{Sj}\Delta^0\boldsymbol{\varphi}_j^{n+\frac{1}{2}} - \Delta^0(\mathbf{M}_{Sj}^H\boldsymbol{\varphi}_j^{n+\frac{1}{2}})\right) + \Delta x^2 V_j\boldsymbol{\varphi}_j^{n+\frac{1}{2}}, \quad (12)$$

where the difference operators are $\Delta^0_{\frac{\Delta x}{2}}\boldsymbol{\varphi}_j^n = \boldsymbol{\varphi}^n_{j+\frac{1}{2}} - \boldsymbol{\varphi}^n_{j-\frac{1}{2}}$, $\Delta^0\boldsymbol{\varphi}_j^n = (\Delta^+ + \Delta^-)\boldsymbol{\varphi}_j^n = \boldsymbol{\varphi}^n_{j+1} - \boldsymbol{\varphi}^n_{j-1}$ and $\boldsymbol{\varphi}_j^{n+\frac{1}{2}} = \frac{\boldsymbol{\varphi}_j^{n+1} + \boldsymbol{\varphi}_j^n}{2}$. Δ_t^+ denotes the forward difference in time.

Just like its continuous counterpart (1), the Crank-Nicolson scheme (12) preserves (in time) the discrete ℓ^2-norm of the whole–space problem and is hence unconditionally stable. This is easily seen by multiplying (12) by $(\boldsymbol{\varphi}_j^{n+\frac{1}{2}})^H$ and summation by parts.

For the scalar Schrödinger equation Arnold [1] derived a DTBC, which is reflection-free on the discrete level and conserves the stability properties of the whole-space Crank-Nicolson scheme. The DTBC has the form of a discrete convolution and the convolution coefficients can be obtained easily by a three-term recurrence formula. We will mimic the derivation of Sec. 3 on a discrete level: To derive the DTBC for (12) we solve the $\mathcal{Z}$-transformed system of difference equations in the exterior domain. Then all its solutions are determined by eigenvalues and eigenvectors, which can be distinguished into decaying and increasing solutions by the absolute value of the involved eigenvalue. We obtain the DTBC by using the fact that the exterior solution decays.

In the exterior space $j \geq J$ ($x_J = x_R$) the parameter matrices are constant and the discrete scheme (12) simplifies to

$$\mathrm{i}\frac{\Delta x^2}{\Delta t}(\boldsymbol{\varphi}_j^{n+1} - \boldsymbol{\varphi}_j^n) = -\mathbf{m}\Delta^+\Delta^-\boldsymbol{\varphi}_j^{n+1/2} + \mathrm{i}\Delta x\mathbf{M}\frac{1}{2}\Delta^0\boldsymbol{\varphi}_j^{n+1/2} + \Delta x^2\mathbf{V}\boldsymbol{\varphi}_j^{n+1/2} \tag{13}$$

for $j \geq J$ and $n \geq 0$. The $\mathcal{Z}$-transformation $\mathcal{Z}\{\boldsymbol{\varphi}_j^n\} = \hat{\boldsymbol{\varphi}}_j(z) := \sum_{n=0}^{\infty} z^{-n}\boldsymbol{\varphi}_j^n$ for $z \in \mathbb{C}$ and $|z| > 1$ transforms (13) to

$$2\mathrm{i}\frac{\Delta x^2}{\Delta t}\frac{z-1}{z+1}\hat{\boldsymbol{\varphi}}_j = -\mathbf{m}\Delta^+\Delta^-\hat{\boldsymbol{\varphi}}_j + \mathrm{i}\Delta x\mathbf{M}\frac{1}{2}\Delta^0\hat{\boldsymbol{\varphi}}_j + \Delta x^2\mathbf{V}\hat{\boldsymbol{\varphi}}_j\,, \qquad j \geq J\,. \tag{14}$$

Lemma 4.1 *For each $z \in \mathbb{C}$ with $|z| > 1$, the $\mathcal{Z}$-transformed exterior problem* (14) *with the boundary data*

$$\hat{\boldsymbol{\varphi}}_{J-1} = \hat{\boldsymbol{\Phi}}\,, \qquad \hat{\boldsymbol{\varphi}}_\infty = 0 \tag{15}$$

has a unique solution.

Proof. As in the proof of Lem. 3.1, we choose $J = 0$, set $\tilde{\boldsymbol{\varphi}}_j := \hat{\boldsymbol{\varphi}}_j - \hat{\boldsymbol{\Phi}}2^{-j-1}$, $j \geq -1$, and define the bounded self-adjoint operator

$$\mathbf{L} := -\frac{1}{\Delta x^2}\mathbf{m}\Delta^+\Delta^- + \frac{\mathrm{i}}{2\Delta x}\mathbf{M}\Delta^0 + \mathbf{V}$$

(with the auxiliary definition $\tilde{\boldsymbol{\varphi}}_{-1} = 0$) on $\ell^2(\mathbb{N}_0, \mathbb{C}^d)$. The discrete BVP (14), (15) is then transformed to

$$\Big(\mathbf{L} - \frac{2\mathrm{i}}{\Delta t}\frac{z-1}{z+1}\mathbf{I}\Big)\tilde{\boldsymbol{\varphi}}_j = \mathbf{f}_j := \Big(\frac{2\mathrm{i}}{\Delta t}\frac{z-1}{z+1}\mathbf{I} + \frac{1}{2\Delta x^2}\mathbf{m} + \frac{3\mathrm{i}}{4\Delta x}\mathbf{M} - \mathbf{V}\Big)\hat{\boldsymbol{\Phi}}2^{-j-1} \quad \in \ell^2(\mathbb{N}_0). \tag{16}$$

$\mathrm{Re}\frac{z-1}{z+1} > 0$ implies $\frac{2\mathrm{i}}{\Delta t}\frac{z-1}{z+1} \in \rho(\mathbf{L})$, and hence (16) has a unique solution $\tilde{\boldsymbol{\varphi}} \in \ell^2(\mathbb{N}_0)$. □

For the explicit calculation of the DTBC we define $\hat{\boldsymbol{\xi}}_j = \Delta^-\hat{\boldsymbol{\varphi}}_j$ and reduce the order of the difference equation (14):

$$\underbrace{\begin{pmatrix} \mathrm{i}\frac{\Delta x}{2}\mathbf{M} & -\mathbf{m} \\ -\mathbf{I} & \mathbf{I} \end{pmatrix}}_{A}\begin{pmatrix}\Delta^+\hat{\boldsymbol{\varphi}}_j \\ \Delta^+\hat{\boldsymbol{\xi}}_j\end{pmatrix} = \underbrace{\begin{pmatrix} \Delta x^2 2\frac{z-1}{z+1}\frac{1}{\Delta t}\mathrm{i}\mathbf{I} - \Delta x^2\mathbf{V} & -\mathrm{i}\frac{\Delta x}{2}\mathbf{M} \\ \mathbf{0} & -\mathbf{I}\end{pmatrix}}_{B}\begin{pmatrix}\hat{\boldsymbol{\varphi}}_j \\ \hat{\boldsymbol{\xi}}_j\end{pmatrix}, \qquad j \geq J\,,$$

i.e.

$$\begin{pmatrix}\Delta^+\hat{\boldsymbol{\varphi}}_j \\ \Delta^+\hat{\boldsymbol{\xi}}_j\end{pmatrix} = \mathbf{A}^{-1}\mathbf{B}\begin{pmatrix}\hat{\boldsymbol{\varphi}}_j \\ \hat{\boldsymbol{\xi}}_j\end{pmatrix} \qquad \text{or} \qquad \begin{pmatrix}\hat{\boldsymbol{\varphi}}_{j+1} \\ \hat{\boldsymbol{\xi}}_{j+1}\end{pmatrix} = (\mathbf{A}^{-1}\mathbf{B} + \mathbf{I})\begin{pmatrix}\hat{\boldsymbol{\varphi}}_j \\ \hat{\boldsymbol{\xi}}_j\end{pmatrix}, \qquad j \geq J\,.$$

The regularity of $\mathbf{A}$ will follow from Lem. 4.5. Solutions of (14), that are constructed with an eigenvalue λ of $\mathbf{A}^{-1}\mathbf{B}$, are decaying for $x \to \infty$ if $|\lambda + 1| < 1$ and increasing if $|\lambda + 1| > 1$. Analogously to Thm. 3.2 we prove a splitting property of $\mathbf{A}^{-1}\mathbf{B} + \mathbf{I}$:

Theorem 4.2 (Discrete Splitting Theorem) *For $|z| \neq 1$, d eigenvalues of $\mathbf{A}^{-1}\mathbf{B} + \mathbf{I}$ are located inside and the other d eigenvalues are outside the unit circle.*

A proof of Thm. 4.2 will be given succeeding to the DTBC at the end of this section.

We may again split the Jordan form $\mathbf{J} = \left(\begin{smallmatrix}\mathbf{J}_1 & \mathbf{0} \\ \mathbf{0} & \mathbf{J}_2\end{smallmatrix}\right)$ of $\mathbf{A}^{-1}\mathbf{B} + \mathbf{I}$, $\mathbf{J}_1 \in \mathbb{C}^{d\times d}$ containing the Jordan blocks corresponding to solutions decaying for $j \to \infty$ and $\mathbf{J}_2$ those which increase. With the matrix of left eigenvectors $\mathbf{P}^{-1} = \left(\begin{smallmatrix}\mathbf{P}_1 & \mathbf{P}_2 \\ \mathbf{P}_3 & \mathbf{P}_4\end{smallmatrix}\right)$ the equation

$$\mathbf{P}^{-1}\begin{pmatrix}\hat{\boldsymbol{\varphi}}_{j+1} \\ \hat{\boldsymbol{\xi}}_{j+1}\end{pmatrix} = \mathbf{P}^{-1}(\mathbf{A}^{-1}\mathbf{B}+\mathbf{I})\begin{pmatrix}\hat{\boldsymbol{\varphi}}_j \\ \hat{\boldsymbol{\xi}}_j\end{pmatrix} = \mathbf{P}^{-1}\mathbf{P}\begin{pmatrix}\mathbf{J}_1 & \mathbf{0} \\ \mathbf{0} & \mathbf{J}_2\end{pmatrix}\begin{pmatrix}\mathbf{P}_1 & \mathbf{P}_2 \\ \mathbf{P}_3 & \mathbf{P}_4\end{pmatrix}\begin{pmatrix}\hat{\boldsymbol{\varphi}}_j \\ \hat{\boldsymbol{\xi}}_j\end{pmatrix} = \begin{pmatrix}\mathbf{J}_1 & \mathbf{0} \\ \mathbf{0} & \mathbf{J}_2\end{pmatrix}\begin{pmatrix}\mathbf{P}_1\hat{\boldsymbol{\varphi}}_j + \mathbf{P}_2\hat{\boldsymbol{\xi}}_j \\ \mathbf{P}_3\hat{\boldsymbol{\varphi}}_j + \mathbf{P}_4\hat{\boldsymbol{\xi}}_j\end{pmatrix}$$

holds and the *transformed discrete transparent boundary conditions* read

$$\mathbf{P}_1^L\hat{\boldsymbol{\varphi}}_1 + \mathbf{P}_2^L\hat{\boldsymbol{\xi}}_1 = 0 \qquad \text{and} \qquad \mathbf{P}_3^R\hat{\boldsymbol{\varphi}}_J + \mathbf{P}_4^R\hat{\boldsymbol{\xi}}_J = 0$$

for the left and right boundary, respectively.

Remark 4.3 In the considered example the matrices $\mathbf{P}_k^R$ and $\mathbf{P}_k^L$ ($k = 1, ..., 4$) were regular, but this is not clear in general.

For regular matrices $\mathbf{P}_4^R$ and $\mathbf{P}_2^L$ the $\mathcal{Z}$-transformed DTBC can be given in Dirichlet-to-Neumann form

$$\Delta^- \hat{\boldsymbol{\varphi}}_1 = \widehat{\mathbf{D}}_L \hat{\boldsymbol{\varphi}}_1 \qquad \text{and} \qquad \Delta^- \hat{\boldsymbol{\varphi}}_J = \widehat{\mathbf{D}}_R \hat{\boldsymbol{\varphi}}_J \,, \tag{17}$$

where $\widehat{\mathbf{D}}_R = -(\mathbf{P}_4^R)^{-1}\mathbf{P}_3^R$ and $\widehat{\mathbf{D}}_L = -(\mathbf{P}_2^L)^{-1}\mathbf{P}_1^L$. After an inverse $\mathcal{Z}$-transformation the DTBCs read

$$\boldsymbol{\varphi}_1^{n+1} - \boldsymbol{\varphi}_0^{n+1} - \mathbf{D}_L^0 \boldsymbol{\varphi}_1^{n+1} = \sum_{k=1}^{n} \mathbf{D}_L^{n+1-k} \boldsymbol{\varphi}_1^k \qquad \text{and} \qquad \boldsymbol{\varphi}_J^{n+1} - \boldsymbol{\varphi}_{J-1}^{n+1} - \mathbf{D}_R^0 \boldsymbol{\varphi}_J^{n+1} = \sum_{k=1}^{n} \mathbf{D}_R^{n+1-k} \boldsymbol{\varphi}_J^k \,. \tag{18}$$

Remark 4.4 Note that in equation (17) and (18) the left boundary condition is given at $j = 1$. Of course, the boundary condition can also be formulated at $j = 0$ using $\Delta^+ \hat{\boldsymbol{\varphi}}_j$.

Ehrhardt and Arnold showed in [14] for a scalar Schrödinger equation that the imaginary parts of their convolution coefficients $\{d_{L,R}^k\}$ were not decaying but oscillating. Therefore they introduced the summed coefficients $\{s_{L,R}^k := d_{L,R}^k + d_{L,R}^{k-1}\}$, which decay like $O(n^{-3/2})$ and hence avoid subtractive cancellation in the evaluation of the convolution. For our coefficient matrices $\{\mathbf{D}_{L,R}^k\}$ it seems difficult to rigorously prove the asymptotic behaviour, but empirically the situation is similar to the scalar case: only the summed coefficients $\{\mathbf{S}_{L,R}^k := \mathbf{D}_{L,R}^k + \mathbf{D}_{L,R}^{k-1}\}$ decay. The DTBCs then read

$$\begin{aligned}
\boldsymbol{\varphi}_1^{n+1} - \boldsymbol{\varphi}_0^{n+1} - \mathbf{S}_L^0 \boldsymbol{\varphi}_1^{n+1} &= \sum_{k=1}^{n} \mathbf{S}_L^{n+1-k} \boldsymbol{\varphi}_1^k - \boldsymbol{\varphi}_1^n + \boldsymbol{\varphi}_0^n \,, \\
\boldsymbol{\varphi}_J^{n+1} - \boldsymbol{\varphi}_{J-1}^{n+1} - \mathbf{S}_R^0 \boldsymbol{\varphi}_J^{n+1} &= \sum_{k=1}^{n} \mathbf{S}_R^{n+1-k} \boldsymbol{\varphi}_J^k - \boldsymbol{\varphi}_J^n + \boldsymbol{\varphi}_{J-1}^n \,.
\end{aligned}$$

It remains to prove the eigenvalue splitting of Thm. 4.2. To this end, we will first show in Lem. 4.5 that no eigenvalue of $\mathbf{A}^{-1}\mathbf{B} + \mathbf{I}$ has an absolute value of one. Then we will show the asserted splitting of the eigenvalues for $\mathbf{M} = 0$ and argue, that due to the continuity of the eigenvalues the border $|\lambda| = 1$ cannot be crossed.

Lemma 4.5 *For $|z| \neq 1$ the matrix $\mathbf{A}^{-1}\mathbf{B} + \mathbf{I}$ has no eigenvalue λ with $|\lambda| = 1$.*

Proof. Assume that $\lambda = a + b\mathrm{i}$ with $|\lambda| = 1$ is an eigenvalue with eigenvector $(\hat{\boldsymbol{\varphi}}_0, \hat{\boldsymbol{\xi}}_0)^\top$ of the discrete problem (14). Then $\hat{\boldsymbol{\varphi}}_j = \lambda^j \hat{\boldsymbol{\varphi}}_0$ is a solution of the discrete problem (14). Inserting $\hat{\boldsymbol{\varphi}}_j = \lambda^j \hat{\boldsymbol{\varphi}}_0$ in equation (14) yields with $g(z) = \frac{z-1}{z+1}$:

$$\mathrm{i}\frac{2\Delta x^2}{\Delta t} g(z) \hat{\boldsymbol{\varphi}}_0 = \left(-\mathbf{m}(a-1) + \mathbf{M}\Delta x b + \Delta x^2 \mathbf{V}\right) \hat{\boldsymbol{\varphi}}_0. \tag{20}$$

Thus, $2\mathrm{i}g(z)\Delta x^2/\Delta t$ is an eigenvalue of the Hermitian matrix $-\mathbf{m}(a-1) + \mathbf{M}\Delta x b + \Delta x^2 \mathbf{V}$. This implies $g(z) \in \mathrm{i}\mathbb{R}$, which holds iff $|z| = 1$. □

To understand the eigenvalue-splitting for equation (14), we shall now use a perturbation argument and consider first the special case $\mathbf{M} = \mathbf{0}$. Then equation (14) reads

$$2\mathrm{i}\frac{\Delta x^2}{\Delta t}\frac{z-1}{z+1}\hat{\boldsymbol{\varphi}}_j = -\mathbf{m}\Delta^+\Delta^-\hat{\boldsymbol{\varphi}}_j + \Delta x^2 \mathbf{V}\hat{\boldsymbol{\varphi}}_j \,. \tag{21}$$

Exchanging the space index $j \to -j$ yields the identical equation. Thus, both problems have the same solutions and the eigenvalues of $\mathbf{A}^{-1}\mathbf{B} + \mathbf{I}$ are the same in both cases. Since decaying solutions are increasing for $j \to -j$ and vice versa, the eigenvalues must split in d yielding decaying and d yielding increasing solutions for $|z| \neq 1$ and $j \to \infty$.

To the r.h.s. of (21) we now add the term $\mathrm{i}\varepsilon\frac{\Delta x}{2}\mathbf{M}(\Delta^+ + \Delta^-)\boldsymbol{\varphi}$ for $0 \leq \varepsilon \leq 1$. Then, Lem. 4.5 shows that no eigenvalue λ of the corresponding matrices $\mathbf{A}_\varepsilon^{-1}\mathbf{B}_\varepsilon + \mathbf{I}$ can have an absolute value one. Since these eigenvalues are continuous in ε, d eigenvalues must remain inside the unit circle when ε varies from 0 to 1 and d eigenvalues stay outside. This finishes the proof of Thm. 4.2.

5 Computation of the Convolution Coefficients by Numerical Inverse $\mathcal{Z}$-Transformation

The $\mathcal{Z}$-transformation (or in the analytical case the Laplace-transformation) enables us to solve the exterior domain equations for deriving transparent boundary conditions. In the implementation the numerical inverse $\mathcal{Z}$-transformation of the convolution coefficients is a subtle problem due to its inherent instabilities.

In this section we will examine the numerical error caused by the inverse $\mathcal{Z}$-transformation, since it is the crucial point in our numerical implementation. First we shall review the inverse $\mathcal{Z}$-transformation: Assume that the $\mathcal{Z}$-transform $hat\ell(z) =$

$\sum_{n=0}^{\infty} \ell_n z^{-n}$ is analytic for $|z| > R \geq 0$. The coefficients are then recovered by $\ell_n = \frac{1}{2\pi i} \oint_{S_\rho} \hat{\ell}(z) z^{n-1} dz$, where S_ρ denotes the circle with radius $\rho > R$. With the substitution $z = \rho e^{i\varphi}$ we have

$$\ell_n = \frac{\rho^n}{2\pi} \int_0^{2\pi} \hat{\ell}\left(\rho \mathrm{e}^{\mathrm{i}\varphi}\right) \mathrm{e}^{\mathrm{i}n\varphi} d\varphi \,. \tag{22}$$

For $\rho = 1$ this shows that the (inverse) $\mathcal{Z}$-transformation is an isometry between $\{\ell_n\} \in \ell^2(\mathbb{N}_0)$ and $\hat{\ell}\big|_{|z|=1} \in L^2(0, 2\pi)$.

For $\rho > 1$, however, the *amplification factors* ρ^n in (22) will be the reason for the numerical instabilities. On the other hand, $\rho = 1$ cannot be chosen either for the application to DTBCs, due to the poor regularity of $\widehat{\mathbf{D}}(z)$ on the unit circle. For the scalar Schrödinger equation, e.g., $\hat{d}(z)$ has two branch-points of type $\sqrt{z^2 - 1}$ (cf. [1], [14]), and hence too many quadrature points would be necessary for the numerical evaluation of (22). But $\hat{d}(z)$ is analytic for $|z| > 1$. So, one has to choose ρ as a compromise between more smoothness of $\hat{\ell}\big|_{|z|=\rho}$ (which allows for an efficient discretisation of (22)), and growing instabilities for large ρ.

For the numerical inverse transformation we choose a radius r and N equidistant sampling points $z_k = r\mathrm{e}^{-\mathrm{i}k2\pi/N}$. The approximate inverse transform,

$$\ell_n^N = \frac{1}{N} r^n \sum_{k=0}^{N-1} \hat{\ell}(z_k)\, \mathrm{e}^{\mathrm{i}nk\frac{2\pi}{N}}, \quad n = 0, \ldots N-1 \tag{23}$$

can then be calculated efficiently by an FFT. The numerical error of ℓ_n^N can be separated into ε_{approx}, the approximation error due to the finite number of sampling points, and the roundoff error ε_{round}, which is amplified by ρ^n. We shall now derive an estimate for this error. Defining $Q_{\hat{\ell}}^\rho = \max\limits_{0 \leq \varphi \leq 2\pi} \left|\hat{\ell}\left(\rho \mathrm{e}^{\mathrm{i}\varphi}\right)\right|$ gives the estimate

$$|\ell_n| \leq \rho^n Q_{\hat{\ell}}^\rho \,. \tag{24}$$

We insert the exact form of $\hat{\ell}_k = \hat{\ell}(z_k)$ into (23), change the order of summation and use the orthogonality property

$$\ell_n^N \;=\; \frac{1}{N} r^n \sum_{m=0}^{\infty} \ell_m r^{-m} \sum_{k=0}^{N-1} \mathrm{e}^{-\mathrm{i}mk\frac{2\pi}{N}} \mathrm{e}^{\mathrm{i}nk\frac{2\pi}{N}} = \frac{1}{N} r^n \sum_{m=0}^{\infty} \ell_m r^{-m} \begin{cases} N & \text{, if } m = n + jN\,, \quad j \in \mathbb{N}_0 \\ 0 & \text{, else} \end{cases} .$$

This gives $\ell_n^N - \ell_n = \sum_{k=1}^{\infty} \ell_{n+kN}\, r^{-kN}$. Here, we insert inequality (24) and sum the geometric series, which yields

$$|\ell_n^N - \ell_n| \leq \rho^n Q_{\hat{\ell}}^\rho \sum_{k=1}^{\infty} \left(\frac{\rho}{r}\right)^{kN} = \rho^n Q_{\hat{\ell}}^\rho \frac{\left(\frac{\rho}{r}\right)^N}{1 - \left(\frac{\rho}{r}\right)^N} \qquad \text{for } r > \rho > R. \tag{25}$$

We remark that similar estimates have been derived in the application of quadrature rules to numerical integration by Lubich, which involve Fourier transformation (cf. [16]).

The other influential error is the roundoff error that depends on the machine accuracy ε_m and the accuracy ε in the numerical computation of $\hat{\ell}_k$. For instance, we will use $\tilde{a} = a(1 + \varepsilon_m)$ as the computer representation of an exact value a. The roundoff error of the inverse $\mathcal{Z}$-transformation is calculated from equation (23). The main part results from the N fold summation of $\hat{\ell}_k$ and the exponential function:

$$\left|\tilde{\ell}_n^N - \ell_n^N\right| \leq r^n \left(CN\varepsilon_m + \varepsilon\right) Q_{\hat{\ell}_k}^r \,.$$

Together with (25) the error is bounded by

$$|\tilde{\ell}_n^N - \ell_n| \leq \rho^n Q_{\hat{\ell}}^\rho \frac{\left(\frac{\rho}{r}\right)^N}{1 - \left(\frac{\rho}{r}\right)^N} + r^n \left((N+1)\varepsilon_m + \varepsilon\right) Q_{\hat{\ell}_k}^r + O(\varepsilon_m^2 + \varepsilon\varepsilon_m) \,. \tag{26}$$

We shall illustrate this error behaviour in a numerical example. We calculated the series $\mathbf{D}^n$ for the quantum well problem with different accuracies (20, 30 and 40 digits precision) and considered the solution obtained with 50 digits precision as a reference solution. We used $N = 256$ sampling points on the circle. The Euclidean norm of the error is shown in Fig. 2(a) for one of the 16 entries in the matrix $\mathbf{D}$. For all entries the error has the same behaviour: the error decreases with growing radius, up to a r_{opt}, after which the roundoff error grows rapidly. Observe, that the y-axis of the plot is in logarithmic scale. The curves for 20, 30 and 40 digits coincide for small values of r up to the radius r_{opt}^{20}, r_{opt}^{30} respectively.

The Fig. 2(a) shows the influence of the mantissa length on the accuracy of the calculation. Next, we want to show the dependence of the error on the number N of sampling points. Fig. 2(b) shows five error curves with 20 digits precision; one

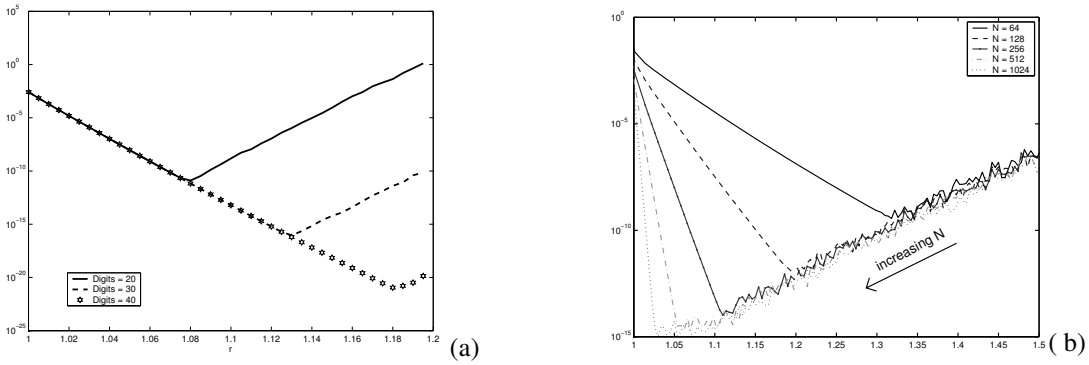

Fig. 2 Error in one element of the matrix $\mathbf{D}$ as a function of the radius r
(a) depending on the number of digits (with $N = 256$ fixed) and
(b) calculated with 20 digits precision depending on the number N of sampling points for the inverse $\mathcal{Z}$-transformation.

for N= 64, 128, 256, 512 and 1024, respectively. The Euclidean norm of the error is summed up to 64. A higher number of sampling points yields a faster decreasing error, r_{opt} becomes smaller and of course the error at r_{opt} becomes less. An influence of N on the round off error is hardly discernable. Comparing the errors at the different N-depending r_{opt}, we notice, that the gain of taking the double number of points gets less with increasing N. Of course the error cannot become less than the precision in the calculation of $\hat{\ell}_n$.

Since the calculation for a system is rather expensive, it is desirable to predict a radius close to r_{opt}. For the different entries in $\mathbf{D}$ the optimal radius varies only slightly - up to a difference of 0.001. We computed the matrices $\hat{\mathbf{D}}$ and $\hat{\mathbf{S}}$ with MATLAB with an accuracy of $\varepsilon = 10^{-16}$. Thus, with a radius $r = 1.018$ and $N = 2^{12}$ sampling points, we achieve an accuracy of 10^{-8}.

6 The Sum-of-Exponentials Ansatz and the Fast Evaluation of the Convolution

In order to reduce the numerical effort of the boundary convolutions (18), it is necessary to make some approximation. We will use the approach of [2] to approximate the coefficients $\widetilde{s}^n_{s,l}$ by the *sum-of-exponentials* ansatz and show a method to evaluate the discrete convolution with the approximated convolution coefficients $\widetilde{a}^n_{s,l}$ efficiently.

6.1 The Sum-of-Exponentials Ansatz

The approximation has to be done for each element in $\mathbf{S}$ separately. We use for each $s, \tau = 1, \ldots, d$ the following ansatz

$$\widetilde{s}^n_{s,\tau} \approx \widetilde{a}^n_{s,\tau} := \begin{cases} \widetilde{s}^n_{s,\tau}, & n = 0, \ldots, \nu - 1 \\ \sum\limits_{l=1}^{L(s,\tau)} g_{s,\tau,l}\, h^{-n}_{s,\tau,l}, & n = \nu, \nu+1, \ldots \end{cases}, \tag{27}$$

where $L(s,\tau) \in \mathbb{N}$ and $\nu \geq 0$ are tuneable parameters. The approximation quality of this sum-of-exponentials ansatz depends on $L(s,\tau)$, ν and the sets $\{g_{s,\tau,l}\}$ and $\{h_{s,\tau,l}\}$ for all $s, \tau = 1, \ldots, d$.

In the following we present a method to calculate these sets for given $L(s,\tau)$ and ν. We consider the formal power series

$$f_{s,\tau}(x) := \widetilde{s}^{\nu}_{s,\tau} + \widetilde{s}^{\nu+1}_{s,\tau} x + \widetilde{s}^{\nu+2}_{s,\tau} x^2 + \ldots\,, \qquad \text{for } |x| \leq 1\,. \tag{28}$$

If the Padé approximation of (28) $\tilde{f}_{s,\tau}(x) := \frac{n^{(L(s,\tau)-1)}_{s,\tau}(x)}{d^{(L(s,\tau))}_{s,\tau}(x)}$ exists (where the numerator and the denominator are polynomials of degree $L(s,\tau)-1$ and $L(s,\tau)$ respectively), then its Taylor series $\tilde{f}_{s,\tau}(x) = \widetilde{a}^{\nu}_{s,\tau} + \widetilde{a}^{\nu+1}_{s,\tau} x + \widetilde{a}^{\nu+2}_{s,\tau} x^2 + \ldots$ satisfies the conditions $\widetilde{a}^n_{s,\tau} = \widetilde{s}^n_{s,\tau}$ for $n = \nu, \nu+1, \ldots, 2L(s,\tau) + \nu - 1$ according to the definition of the Padé approximation rule.

We now explain, how to compute the coefficient sets $\{g_{s,\tau,l}\}$ and $\{h_{s,\tau,l}\}$.

Theorem 6.1 ([2]**, Theorem 3.1.)** *Let $d^{L(s,\tau)}_{s,\tau}$ have $L(s,\tau)$ simple roots $h_{s,\tau,l}$ with $|h_{s,\tau,l}| > 1$, $l = 1, \ldots, L(s,\tau)$. Then*

$$\widetilde{a}^n_{s,\tau} = \sum_{l=1}^{L(s,\tau)} g_{s,\tau,l}\, h^{-n}_{s,\tau,l}\,, \qquad n = \nu, \nu+1, \ldots,$$

where

$$g_{s,\tau,l} := -\frac{n^{(L(s,\tau)-1)}_{s,\tau}(h_{s,\tau,l})}{\big(d^{(L(s,\tau))}_{s,\tau}\big)'(h_{s,\tau,l})}\, h^{\nu-1}_{s,\tau,l} \neq 0\,, \qquad l = 1, \ldots, L(s,\tau)\,.$$

Remark 6.2 The asymptotic decay of the $\widetilde{a}^n_{s,\tau}$ is exponential. This is due to the sum-of-exponentials ansatz (27) and the assumption $|h_{s,\tau,l}| > 1, l = 1, \ldots, L(s,\tau)$.

The above analysis permits us to give the following description of the approximation to the convolution coefficients by the representation (27) if we use a $[L(s,\tau)-1|L(s,\tau)]$ Padé approximant to (28): the first $2L(s,\tau)+\nu-1$ coefficients are reproduced exactly; however, the asymptotic behaviour of $\widetilde{s}^n_{s,\tau}$ and $\widetilde{a}^n_{s,\tau}$ (as $n \to \infty$) differs strongly (algebraic versus exponential decay).

We note that the Padé approximation must be performed with high precision ($2L(s,\tau)-1$ digits mantissa length) to avoid a 'nearly breakdown' by ill conditioned steps in the Lanczos algorithm. If such problems still occur or if one root of the denominator is smaller than 1 in absolute value, the orders of the numerator and denominator polynomials are successively reduced. In our numerical test case we started with $L(s,\tau) \equiv 30$ and except from two outlier values the finally reached values of $L(s,\tau)$ were between 25 and 30. Figure 3 shows the error $|\widetilde{s}^n_{s,\tau} - \widetilde{a}^n_{s,\tau}|$ versus n for the outlier with $L(1,2) = 15$ for the imaginary part of $\widetilde{s}^n_{1,2}$ (a) and with $L(2,2) = 30$ for the real part of $\widetilde{s}^n_{2,2}$ (b). Observe, that both plots are in logarithmic scale. Clearly, the error increases significantly for $n > 2L(s,\tau)+1$.

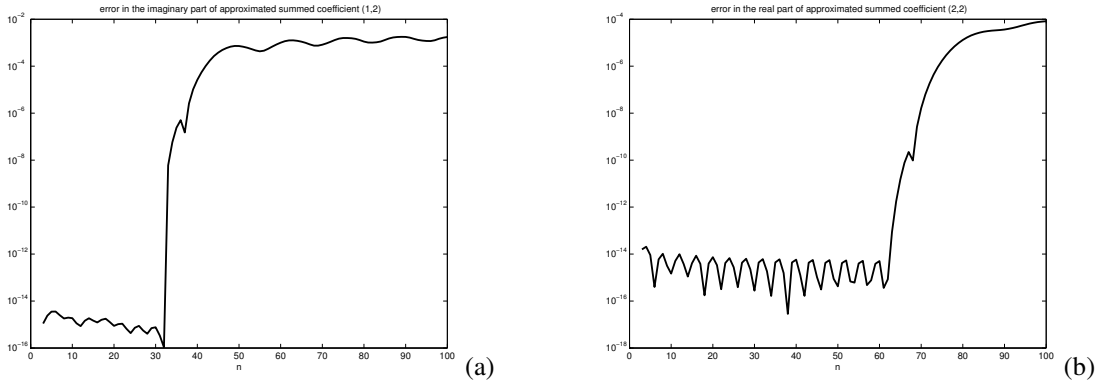

(a) (b)

Fig. 3 Error $|\widetilde{s}^n_{s,\tau} - \widetilde{a}^n_{s,\tau}|$ versus n: imaginary part (a) for $s = 1$, $\tau = 2$ and (b) real part for $s = \tau = 2$.

6.2 The Fast Evaluation of the Approximate Convolution

Now we describe the fast evaluation of the discrete approximate convolution. The convolution

$$C^{(n+1)}_{s,\tau}(u) := \sum_{k=1}^{n+1-\nu} \widetilde{a}^{n+1-k}_{s,\tau}\, u^k_{\tau,J}\,, \qquad \text{with } \widetilde{a}^n_{s,\tau} := \sum_{l=1}^{L(s,\tau)} g_{s,\tau,l}\, h^{-n}_{s,\tau,l}, \qquad n = \nu, \nu+1, \ldots$$

can be calculated efficiently by a simple recurrence formula:

Theorem 6.3 ([2]**, Theorem 4.1.)**

$$C^{(n+1)}_{s,\tau}(u) = \sum_{l=1}^{L(s,\tau)} C^{(n+1)}_{s,\tau,l}(u) \tag{29}$$

with

$$\begin{aligned} C^{(n+1)}_{s,\tau,l}(u) &= h^{-1}_{s,\tau,l} C^{(n)}_{s,\tau,l} + g_{s,\tau,l} h^{-\nu}_{s,\tau,l} u^{n+1-\nu}_{\tau,J}\,, \qquad n = \nu, \nu+1, \ldots \\ C^{(\nu)}_{s,\tau,l}(u) &\equiv 0\,. \end{aligned} \tag{30}$$

6.3 Summary of the Proposed Method to Evaluate Approximate DTBCs

Step 1: For each s, τ choose $L(s,\tau)$ and ν and calculate the exact convolution coefficients $\widetilde{s}^n_{s,\tau}$ for $n = 0, \ldots, 2L(s,\tau)+\nu-1$.

Step 2: For each s, τ use the Padé approximation for the Taylor series with $\widetilde{a}^n_{s,\tau} = \widetilde{s}^n_{s,\tau}$, for $n = \nu, \nu+1, \ldots, 2L(s,\tau)+\nu-1$ to calculate the sets $\{g_{s,\tau,l}\}$ and $\{h_{s,\tau,l}\}$ for all $s, \tau = 1, \ldots, d$ according to Theorem 6.1.

Step 3: Implement the recurrence formulas (29), (30) to calculate the approximate convolutions.

7 Numerical Results

In this section we present the numerical results for simulating the transient behaviour of the quantum well with the data of Sect. 2.1. We choose the discretisation parameters $\Delta x = 1/20$, $\Delta t = 0.015$ for the computational domain $[-12, 5]$ and compute the convolution coefficients of the DTBC as described in Sec. 6. First, to study the behaviour of the DTBC, we present a system of Schrödinger equations with zero potential. As initial condition we use the Gaussian wave packet of heavy and light holes (2) stimulating a slow and a fast eigenmode. Fig. 4 shows the time-dependent behaviour of the first two components φ_1 (solid) and φ_2 (dashed). We concentrate on the first two components, since there is less mass in component three and four. The density oscillates between the components, moves to the right, fragments in two and the faster wave packet leaves the domain of computation without any visible reflections.

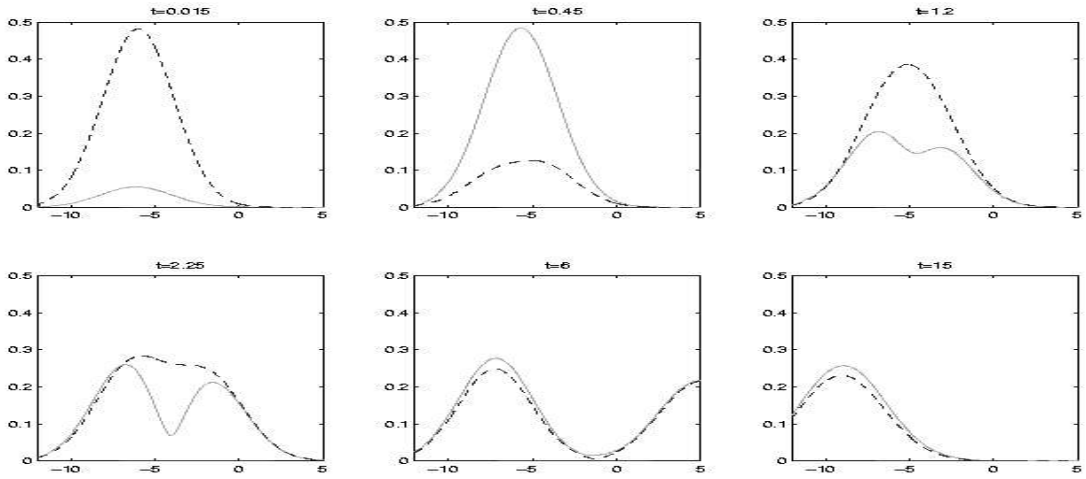

Fig. 4 Time-dependent behaviour of φ_1 (solid) and φ_2 (dashed) for a free Schrödinger system.

Next we consider only the faster mode and add the DBSQW structure (3). When the wave packet reaches the first barrier, it is partly reflected and partly transmitted. With advancing time some part of the density accumulates between the barriers and is slowly transmitted through the second barrier, then leaving the domain of computation. The part of the density, which is reflected at the first barrier moves on to the left and after some time most part of the solution leaves the computational domain in a packet. The wave packet does not recompose smoothly.

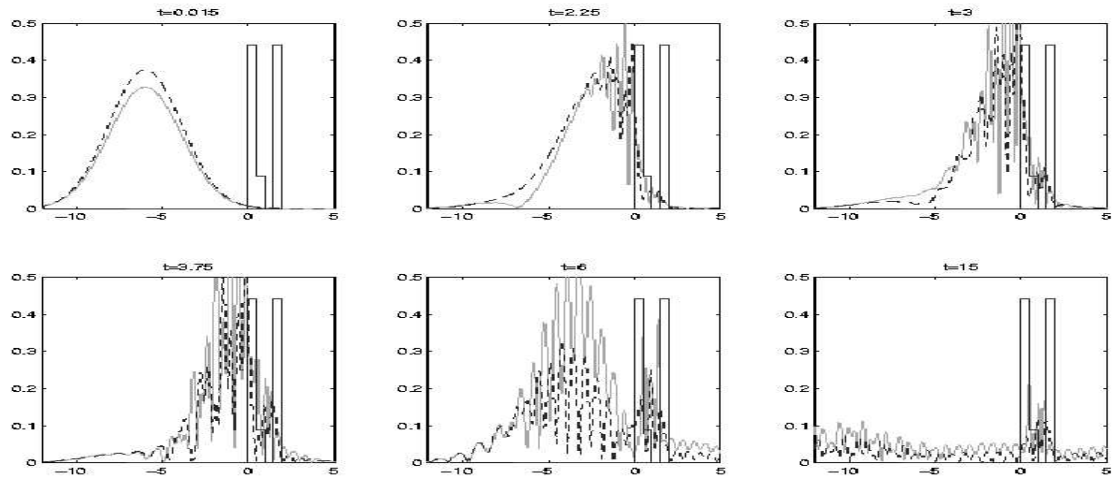

Fig. 5 Time-dependent behaviour of φ_1 (solid) and φ_2 (dashed) for a system with DBSQW structure.

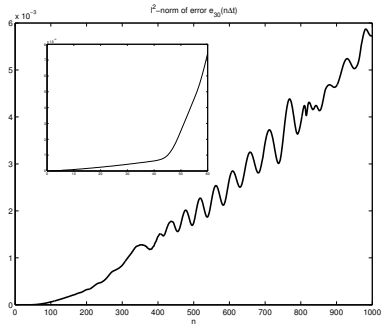

Fig. 6 ℓ^2-error of the solution with approximated coefficients.

In Fig. 6 we present the relative ℓ^2–error $e_L(t) = \|\boldsymbol{\varphi} - \boldsymbol{\varphi}_a\|_2 / \|\boldsymbol{\varphi}(.,0)\|_2$, where $\boldsymbol{\varphi}_a$ denotes the approximate solution obtained with the approximated DTBCs. $\boldsymbol{\varphi}$ is the solution calculated with exact DTBCs. In our example we used $L(s,\tau) = 30$ initially. One observes that the error is increasing in time (due to the interaction with the potential) but remains after 1000 time steps below $6 \cdot 10^{-3}$. The zoomed region shows the ℓ^2-error of the solution for the first 60 time steps, where the upper bound is 10^{-5}.

8 Conclusions and Perspectives

In this paper we showed the mathematical background for a discrete transparent boundary condition for one-dimensional kp-Schrödinger equations in detail and approximated the DTBC by a sum-of-exponentials ansatz. We illustrated by a simple example the quality of these DTBCs. In a succeeding paper, we will concentrate on the analysis of the tunnelling properties of a real quantum-well structure using this tool and calculating physical parameters as charging and escape times.

Acknowledgements The first and third author were supported by the DFG Research Center MATHEON "Mathematics for key technologies" in Berlin. The first two authors were partially supported by the DFG Priority Program Analysis, Modeling and Simulation of Multi-Scale Problems under Grant-No. AR 277/3-2. Th. Koprucki was supported by the same DFG Priority Program under Grant FU 316/5-2.

References

[1] A. Arnold, Numerically Absorbing Boundary Conditions for Quantum Evolution Equations. *VLSI Design* **6**, 313–319 (1998).
[2] A. Arnold, M. Ehrhardt, I. Sofronov, Discrete transparent boundary conditions for the Schrödinger equation: Fast calculation, approximation, and stability. Comm. Math. Sci. **1**, 501–556 (2003).
[3] U. Bandelow, H.-Chr. Kaiser, Th. Koprucki, J. Rehberg, Spectral properties of $k \cdot p$ Schrödinger operators in one space dimension. Numer. Funct. Anal. Opt. **21**, 379–409 (2000).
[4] G. Bastard, Wave Mechanics Applied to Semiconductor Heterostructures (Hasted Press, 1988).
[5] A.C. Rodrigues Bittencourt, A.M.Cohen, G.E. Marques, Strain-indused enhancement of resonant current of holes in multilayered heterostructures. Phys. Rev. B **57**, 4525–4543 (1998).
[6] M. G. Burt, The justification for applying the effective-mass approximation to microstructures. J. Physics. Condens. Matter **4**, 6651–6690 (1992).
[7] M. G. Burt, Fundamentals of envelope function theory for electronic states and photonic modes in nanostructures. J. Physics. Condens. Matter **11**, R53–R83 (1998).
[8] M. Cardona, Fundamentals of Semiconductors (Springer-Verlag, Berlin, 1996).
[9] D. Carlson, H. Schneider, Inertia theorems for matrices: The semidefinite case. J. Math. Anal. Appl. **6**, 430–446 (1963).
[10] C. Y.-P. Chao, S. L. Chuang, Spin-orbit-coupling effects on the valence-band structure of strained semiconductor quantum wells. Phys. Rev. B **46**, 4110–4122 (1992).
[11] S. L. Chuang, Efficient band-structure calculations of strained quantum wells. Phys. Rev. B **43**, 9649–9661 (1991).
[12] S. L. Chuang, Physics of optoelectronic Devices (Wiley & Sons, New York, 1995).
[13] P. Debernardi, P. Fasano, Quantum Confined Stark Effect in Semiconductor Quantum Wells Including Valence Band Mixing and Coulomb Effects. IEEE J. Quantum Electronics **29**, 2741–2755 (1993).
[14] M. Ehrhardt, A. Arnold, Discrete transparent boundary conditions for the Schrödinger equation. Riv. Mat. Univ. Parma **6**, 57–108 (2001).
[15] E. O. Kane, Energy Band Theory. In W. Paul, editor, Handbook on Semiconductors Vol. 1, chap. 4a, pp. 193–217 (North-Holland, Amsterdam, New York, Oxford, 1982).
[16] C. Lubich, Convolution Quadrature and Discretized Operational Calculus II. Numer. Math. **52**, 413–425 (1988).
[17] A. T. Meney, Besire Gonul, E. P. O'Reilly, Evaluation of various approximations used in the envelope-function method. Phys. Rev. B **50**, 10893–10904 (1994).
[18] M. Reed, B. Simon, Methods of Modern Mathematical Physics 2.Vol.. (Academioc Press, San Diego, 1975).
[19] V. Sankaran, J. Singh, Formalism for tunneling of mixed-symmetry electronic states: Application to electron and hole tunneling in direct- and indirect-band-gap $GaAs/Al_xGa_{1-x}As$ structures. Phys. Rev. B **44**, 3175–3186 (1991).
[20] J. Singh, Physics of semiconductors and their heterostructures. (McGraw–Hill, New York, 1993).
[21] C. Sirtori, P. Kruck, S. Barbieri, Ph. Collot, J. Nagle, M. Beck, J. Faist, U. Oesterle, $GaAs/Al_xGa_{1-x}As$ quantum cascade lasers. Appl. Phys. Lett. **73**, 3486–3488 (1998).
[22] J.A. Stovneng, E.H. Hauge, Time-dependent resonant tunneling of wave packets in the tight-binding model. Phys. Rev. B **44** 13582–13594 (1991).
[23] M. Wagner, H. Mizuta, Complex-energy analysis of intrinsic lifetimes of resonances in biased multiple quantum wells. Phys. Rev. B **48**, 14393–14406 (1993).
[24] J. Zhang, B. Gu, Temporal characteristics of electron tunneling in double-barrier stepped quantum-well structures. Phys. Rev. B **43**, 5028–5034 (1991).
[25] A. Zisowsky, Discrete Transparent Boundary Conditions for Systems of Evolution Equations, Ph.D. thesis, TU Berlin (2003).